AD-A189 863 QUANTUM MONTE CARLO STUDY OF THE NIES ASSOCIATED WITH N2 (X 1 SIGMA SUB G..(U) CALIFORNIA UNIV BERKELEY LAWRENCE BERKELEY LAB W A LESTER OCT 87 AFAL-TR-87-075 1/1

UNCLASSIFIED F/G 20/10 NL

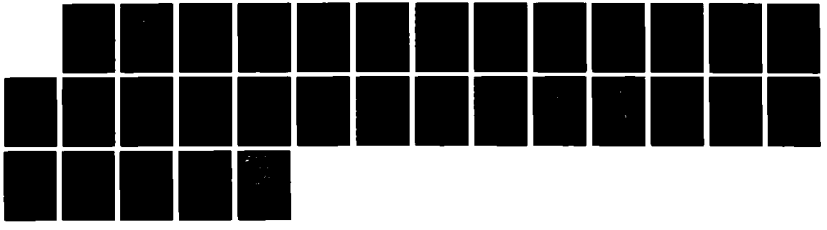

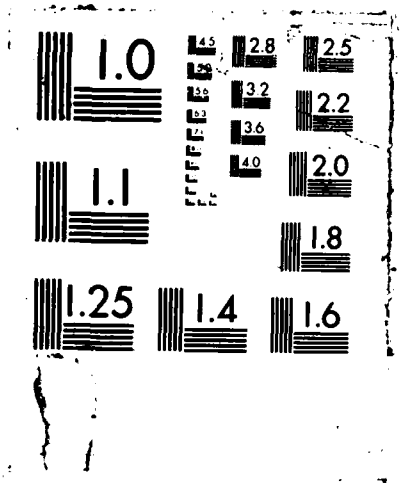
1.0
1.1
1.25
1.4
1.6
1.8
2.0
2.2
2.5
2.8
3.2
3.6
4.0

AFAL-TR-87-075 AD:

Final Report
for the period
1 July 1985 to
30 June 1987

Quantum Monte Carlo Study of the MIES Associated with $H_2(X\ ^1\Sigma_g^+)$ and $H_2\ (B\ ^1\Sigma_u^+)$

October 1987

Author:
W. A. Lester

Lawrence Berkeley Laboratory
University of California
Berkeley, CA 94720

AFRPL 69022

Approved for Public Release

prepared for the: **Air Force Astronautics Laboratory**

Air Force Space Technology Center
Space Division, Air Force Systems Command
Edwards Air Force Base,
California 93523-5000

NOTICE

When U.S. Government drawings, specifications, or other data are used for any purpose other than a definitely related government procurement operation, the government thereby incurs no responsibility nor any obligation whatsoever, and the fact that the government may have formulated, furnished, or in any way supplied the said drawings, specifications, or other data, is not to be regarded by implication or otherwise, or conveying any rights or permission to manufacture, use, or sell any patented invention that may in any way be related thereto.

FOREWORD

This final report was prepared by the Lawrence Berkeley Laboratory in completion of procurement instrument number AFRPL 69022 with the Air Force Astronautics Laboratory (AFAL), Edwards Air Force Base, CA. The period of the report is 1 July 1985 to 30 June 1987. AFAL Project Manager was Dr Steve Rodgers.

This technical report has been reviewed and is approved for distribution in accordance with the the distribution statement on the cover and on the DD Form 1473.

Stephen L. Rodgers

STEPHEN L. RODGERS
Project Manager

FOR THE COMMANDER

ROBERT C. CORLEY
Chief, ARIES Office

SECURITY CLASSIFICATION OF THIS PAGE

REPORT DOCUMENTATION PAGE

1a. REPORT SECURITY CLASSIFICATION UNCLASSIFIED	1b. RESTRICTIVE MARKINGS
2a. SECURITY CLASSIFICATION AUTHORITY	3. DISTRIBUTION/AVAILABILITY OF REPORT Approved for Public Release, Distribution is Unlimited.
2b. DECLASSIFICATION/DOWNGRADING SCHEDULE	
4. PERFORMING ORGANIZATION REPORT NUMBER(S)	5. MONITORING ORGANIZATION REPORT NUMBER(S) AFAL-TR-87-075
6a. NAME OF PERFORMING ORGANIZATION Lawrence Berkeley Laboratory 6b. OFFICE SYMBOL (If applicable)	7a. NAME OF MONITORING ORGANIZATION Air Force Astronautics Laboratory
6c. ADDRESS (City, State and ZIP Code) Lawrence Berkeley Laboratory University of California Berkeley, CA 94720	7b. ADDRESS (City, State and ZIP Code) AFAL/CX Edwards Air Force Base, CA 93523-5000
8a. NAME OF FUNDING/SPONSORING ORGANIZATION 8b. OFFICE SYMBOL (If applicable)	9. PROCUREMENT INSTRUMENT IDENTIFICATION NUMBER AFRPL 69022
8c. ADDRESS (City, State and ZIP Code)	10. SOURCE OF FUNDING NOS.

PROGRAM ELEMENT NO.	PROJECT NO.	TASK NO.	WORK UNIT NO
61101F	5730N	00	TQ

11. TITLE (Include Security Classification) Quantum Monte Carlo Study of the MIES Associated with $H_2(X\ ^1\Sigma_g^+)$

12. PERSONAL AUTHOR(S)
Lester, William A.

13a. TYPE OF REPORT	13b. TIME COVERED	14. DATE OF REPORT (Yr., Mo., Day)	15. PAGE COUNT
Final	FROM 85/7/1 TO 87/6/30	87/10	30

16. SUPPLEMENTARY NOTATION

17 COSATI CODES			18. SUBJECT TERMS (Continue on reverse if necessary and identify by block number)
FIELD	GROUP	SUB. GR.	Tetrahydrogen, multiconfiguration self-consistent-field, quantum Monte Carlo, metastable molecules.
07	04		

19. ABSTRACT (Continue on reverse if necessary and identify by block number)

Initial efforts to characterize the electronically excited state of H_4 that correlates in one asymptotic limit to $H_2(X\ ^1\Sigma_g^+)$ + $H_2(B\ ^1\Sigma_u^+)$ are described. Multiconfiguration self consistent field (MCSCF) and fixed-node quantum Monte Carlo (FNQMC) methods have been used to explore the suggested region of stability. The minimum on the excited-state potential energy surface for pyramidal geometries is found to have an isosceles base. Initial estimates of nonadiabatic coupling matrix elements needed for the determination of lifetimes and stability are determined using normal mode distortions.

20. DISTRIBUTION/AVAILABILITY OF ABSTRACT	21. ABSTRACT SECURITY CLASSIFICATION
UNCLASSIFIED/UNLIMITED ☒ SAME AS RPT ☐ DTIC USERS ☐	UNCLASSIFIED

22a. NAME OF RESPONSIBLE INDIVIDUAL	22b. TELEPHONE NUMBER (Include Area Code)	22c. OFFICE SYMBOL
Stephen L. Rodgers	(805) 275-5413	CX

DD FORM 1473, 83 APR EDITION OF 1 JAN 73 IS OBSOLETE

SECURITY CLASSIFICATION OF THIS PAGE

11. (continued) and H_2 ($B\ ^1\Sigma_u^+$).

TABLE OF CONTENTS

SECTION	PAGE
Introduction	1
Quantum Monte Carlo	3
MCSCF Study of Trigonal Pyramidal Ground-and Excited-State H_4	6
FNQMC Study of the Ground-State Pyramidal Structure for C_{3v} Symmetry	11
FNQMC Study of the Excited State	11
SA-MCSCF Study of Distorted Geometries	15
Nonadiabatic Coupling	20
References	24

List of Figures

Page

Figure 1. Correlation diagram for H_4. 2

Figure 2. MIES coordinate system (assuming C_{3v} symmetry). 7

Figure 3. Ground- and excited-state H_4 potential energy curves for trigonal pyramidal geometry. 8

Figure 4. Potential energy curves from MCSCF trial functions for trigonal pyramidal geometry and C_{3v} symmetry (r = 1.70 a.u.). 9

Figure 5. Geometries used to calculate an approach of H_2(B) to H_2(X). 10

Figure 6. Plot of total energies corresponding to the pathway presented in Fig. 5. 12

Figure 7. Change of charge distribution between H_a and H_b as a function of d, the displacement of the midpoint of H_2(B) above the plane of H_2(X). 13

Figure 8. Potential energy of trigonal pyramidal H_4 versus R. 14

Figure 9. MIES coordinate system used for geometry variation. 16

Figure 10. Potential energy surfaces for the ground- and excited-state separately for easy visualization and in computed relative positioning. 17

Figure 11. Potential energy contour map for R = 4.0 a.u. as a function of a and b. 18

Figure 12. Same as Fig. 11 for R = 3.8 a.u. 19

Figure 13. Potential energy curves for selected R (in a.u.) vs d. 20

Figure 14. Normal mode displacement of H_4 in C_{3v} symmetry. 21

Figure 15. CI contribution to coupling matrix elements for normal mode displacement. 23

INTRODUCTION

Excited states of interacting systems, that are bound in the ground state only by van der Waals forces, can interact to form strongly bound species. This is found even for systems in which only one of the fragments is excited, and is exemplified by the excimer states He-He*, Ar-Ar*, and H_2-H_2^*. Here the asterisk denotes the first excited state of the same spin symmetry as the ground state. Interest in the latter system has increased recently with the study of Nicolaides, Theodorakopoulos, and Petsalakis (NTP)[1] of the $H_2(X\ ^1\Sigma_g^+)$ $H_2(B\ ^1\Sigma_u^+)$ system because of the ionic character of the B state which these authors label at $4.0a_0$, where charge transfer occurs, a maximum ionicity excited states (MIES); see Fig. 1 for the correlation diagram. This state is of special interest because of its strong electrostatic binding.

A model[1-3] based on MIES properties suggests that bound excited states of polyatomic systems can be formed in regions characterized by an avoided crossing with the ground state, if one of the interacting molecules can exist in a MIES. The description for H_2 H_2^*, where H_2^* denotes $H_2(B\ ^1\Sigma_u^+)$ is one in which a positive ion complex H_3^+ is formed, and interacts in its ground state equilibrium geometry (equilateral triangle with $r = 1.65a_0$) with H . The MIES geometry corresponding to H^+ H^- for the parent $H_2(B\ ^1\Sigma_u^+)$ is the charge transfer region at $4.0a_0$. The mechanism supported by NTP with CI computations is one of H_3^+, which is electron deficient in the center of the triangle, interacting with H at a distance of roughly $1.0a_0$ above the plane of the H_3^+ triangle.

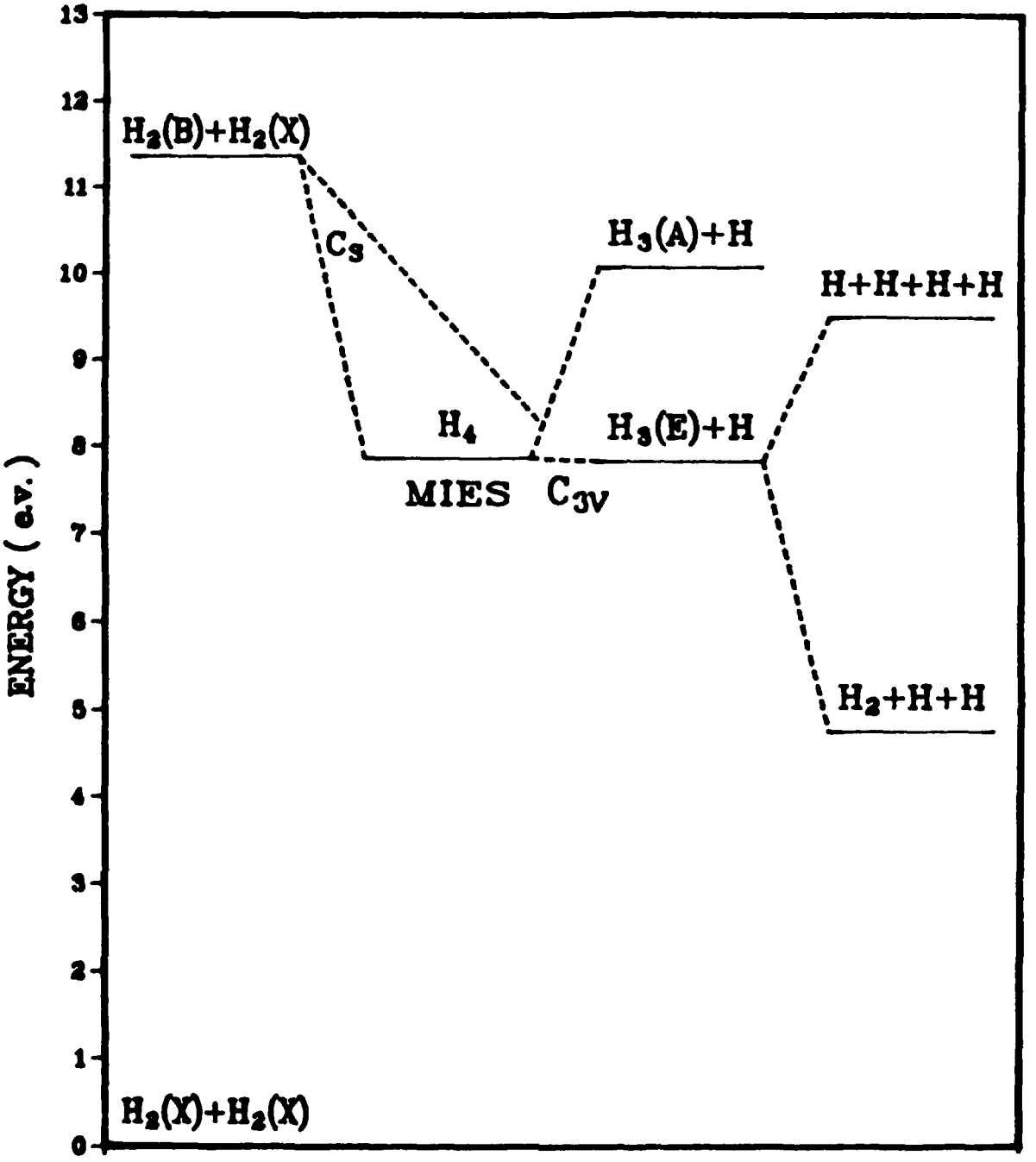

Figure 1. Correlation diagram for H_4.

During the contract period studies of the H_2^+-H_2 system have been pursued in this laboratory using the fixed-node quantum Monte Carlo (FNQMC) method. A brief introduction to the method is presented and followed by a description of FNQMC and other calculations of the subject system.

QUANTUM MONTE CARLO

Monte Carlo approaches to solving problems with many degrees of freedom are a class of statistical methods having in common the generation of "random" numbers. In the past few years, Monte Carlo approaches have seen increased application in a number of diverse fields. What we mean here by quantum Monte Carlo (QMC) is a Monte Carlo procedure which solves the Schrödinger equation. This is to be distinguished from so-called variational Monte Carlo, in which one obtains expectation values for a *given* trial wave function.

This ability to stochastically solve the Schrödinger equation provides an alternative to conventional techniques of quantum chemistry. Early work[4] has shown that highly accurate total energies and correlation energies can be obtained by QMC. In fact, in a procedurally simple manner, accuracies exceeding those of the best *ab initio* configuration interaction calculations have been obtained.

The essence of the procedure is to simulate a quantum system by allowing it (and an ensemble of differently prepared systems) to evolve under the time-dependent Schrödinger equation in imaginary time. Excited states of the same symmetry as a lower state can also be computed with the method.

By writing the imaginary-time Schrödinger equation with a shift in the zero of energy as

$$\frac{\partial \Psi(\underline{R},t)}{\partial t} = D\nabla^2\Psi(\underline{R},t) + [E_T - V(\underline{R})]\Psi(\underline{R},T), \tag{1}$$

we see that it may be interpreted as a generalized diffusion equation. The first term on the right-hand side is the ordinary diffusion term, while the second term is a position-dependent rate (or branching) term. For an electronic system, $D = \hbar^2/2m_e$, $\underline{R}$ is the three-N dimensional coordinate vector of the N electrons, and $V(\underline{R})$ is the Coulomb potential. Since diffusion is the continuum limit of a random walk, one may simulate Eq. (1) with the function Ψ (note, not Ψ^2) as the density of "walks". The walks undergo an exponential birth and death as given by the rate term.

The steady-state solution to Eq. (1) is the time-independent Schrödinger equation. Thus we have $\Psi(\underline{R},t) \rightarrow \phi(\underline{R})$, where ϕ is an energy eigenstate. The value of E_T at which the population of walkers is asymptotically constant gives the energy eigenvalue. Early calculations employing Eq. (1) in this way were done by Anderson on a number of one- to four-electron systems.[5]

In order to treat systems larger than two electrons, the Fermi nature of the electrons must be taken into account. The antisymmetry of the eigenfunction implies that Ψ must change sign; however, a density (e.g., of walkers) cannot be negative. The method which imposes antisymmetry, and at the same time provides efficient sampling (thereby reducing the statistical "noise"), is importance sampling with an antisymmetric trial function Ψ_T. The zeroes (nodes) of Ψ_T become absorbing boundaries for the diffusion process, which maintains the

antisymmetry. The additional boundary condition that Ψ vanish at the nodes of Ψ_T is the fixed-node approximation. The magnitude of the error thus introduced depends on the accuracy of the *nodes* of $\Psi_T(R)$, and vanishes as Ψ_T approaches the true eigenfunction. To the extent that Ψ_T is a good approximation of the wave function, the true eigenfunction is almost certainly quite small near the nodes of Ψ_T. Thus one expects the fixed-node error to be small for reasonable choices of Ψ_T.

To implement importance sampling and the fixed-node approximation, Eq. (1) is multiplied on both sides by Ψ_T, and rewritten in terms of the new probability density $f(\underline{R},t) = \Psi_T(\underline{R})\Psi(\underline{R},t)$. The resultant equation for $f(\underline{R},t)$ may be written

$$\frac{\partial f}{\partial t} = D\nabla^2 f + [E_T - E_L(\underline{R})]f - D\nabla\cdot[fF_Q(\underline{R})]. \tag{2}$$

The local energy $E_L(\underline{R})$, and the "quantum force" $F_Q(\underline{R})$ are simple functions of Ψ_T given by

$$E_L(\underline{R}) \equiv H\Psi_T(\underline{R})/\Psi_T(\underline{R}), \tag{3a}$$

and

$$F_Q(\underline{R}) \equiv 2\nabla\Psi_T(\underline{R})/\Psi_T(\underline{R}). \tag{3b}$$

Equation (2), like Eq. (1) is a generalized diffusion equation, though now with the addition of a drift term due to the presence of F_Q.

In order to perform the random walk implied by Eq. (2) we use a short-time approximation to the Green's function which is used to evolve $f(\underline{R},t) \cdot f(R', t+\tau)$. This evolution process is iterated to large t. The Green's function becomes exact in the limit of vanishing time-step size, τ.

MCSCF PILOT STUDY OF [illegible] PYRAMIDAL GROUND AND EXCITED STATE H_4

[illegible]

MCSCF [illegible] including the [illegible] as H separated [illegible] for R = 3.8 a.u. [illegible] for R = 3.8 a.u. For C_s symmetry the [illegible] the MCSCF pilot [illegible] reflect the better [illegible] the compact MCSCF [illegible] key comparison, however, will be with the DNQMC results obtained with the MCSCF functions. We [illegible] for future interactions.

MCSCF PILOT STUDY OF THE H + H_2(X) → H/B[illegible] H_4 MIES PATHWAYS

Calculations were carried out for the H/B approach to H_2(X) in which these molecules are contained initially in perpendicular planes that bisect each other. Figure 5 depicts the [illegible] and in the accompanying table a sequence of geometry [illegible] that carry the system from the

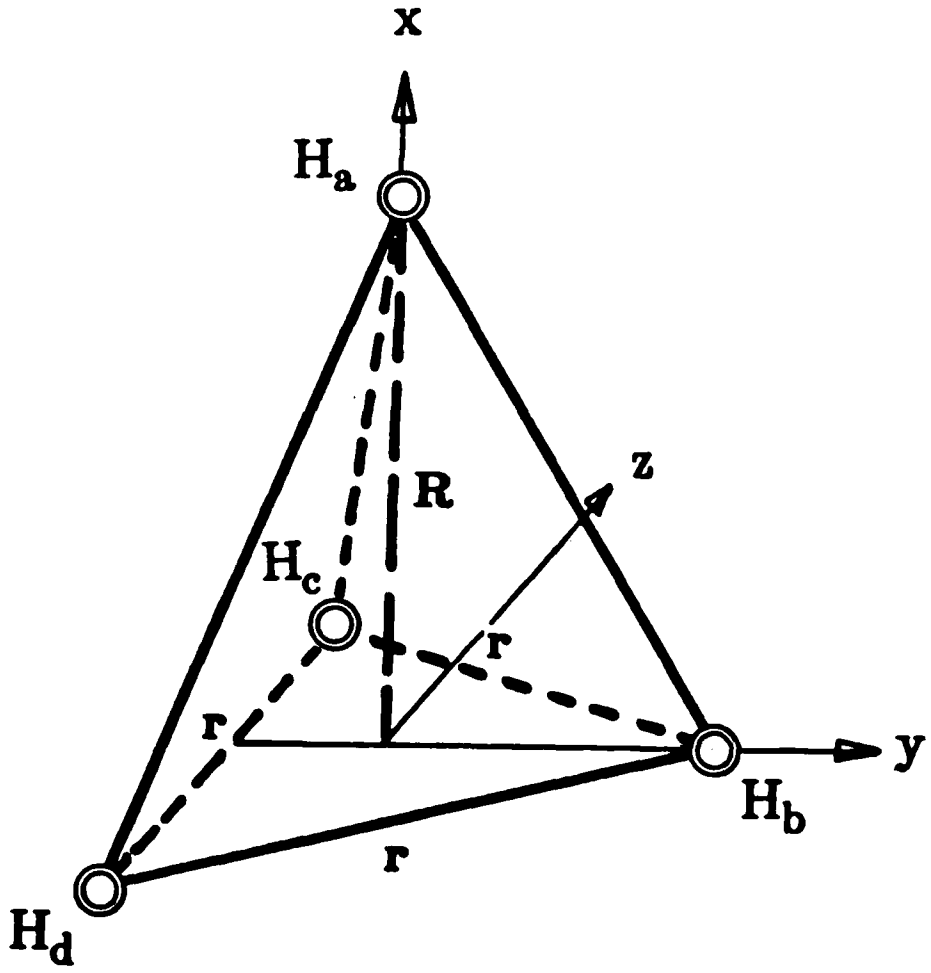

Figure 2. MIES coordinate system (assuming C_{3v} symmetry): R is the distance from H_a to plane of $H_bH_cH_d$ equilateral triangle of side r.

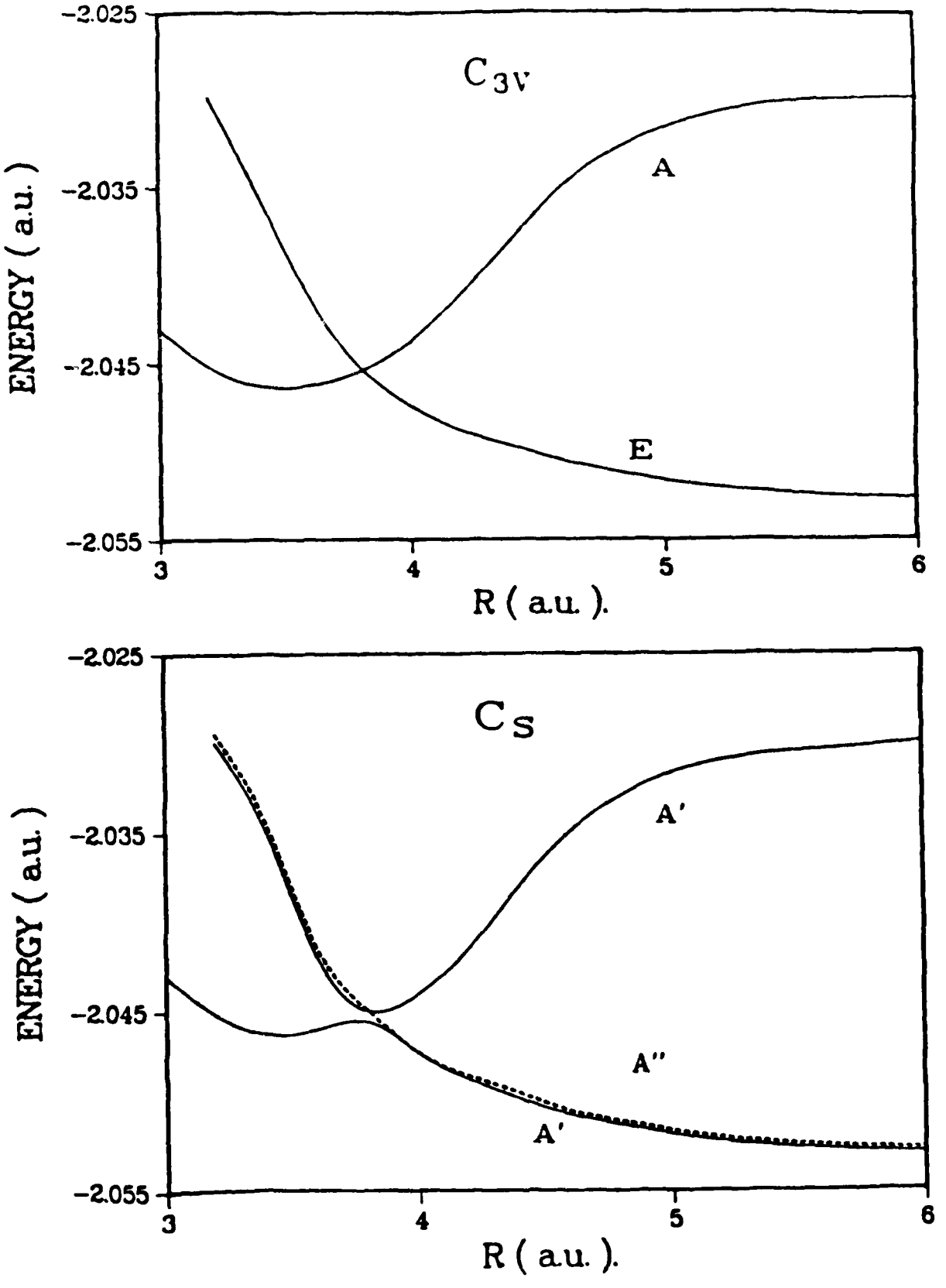

Figure 3. Ground and excited state H_4 potential energy curves for trigonal pyramidal geometry: upper panel (C_{3v} symmetry), lower panel (C_s symmetry).

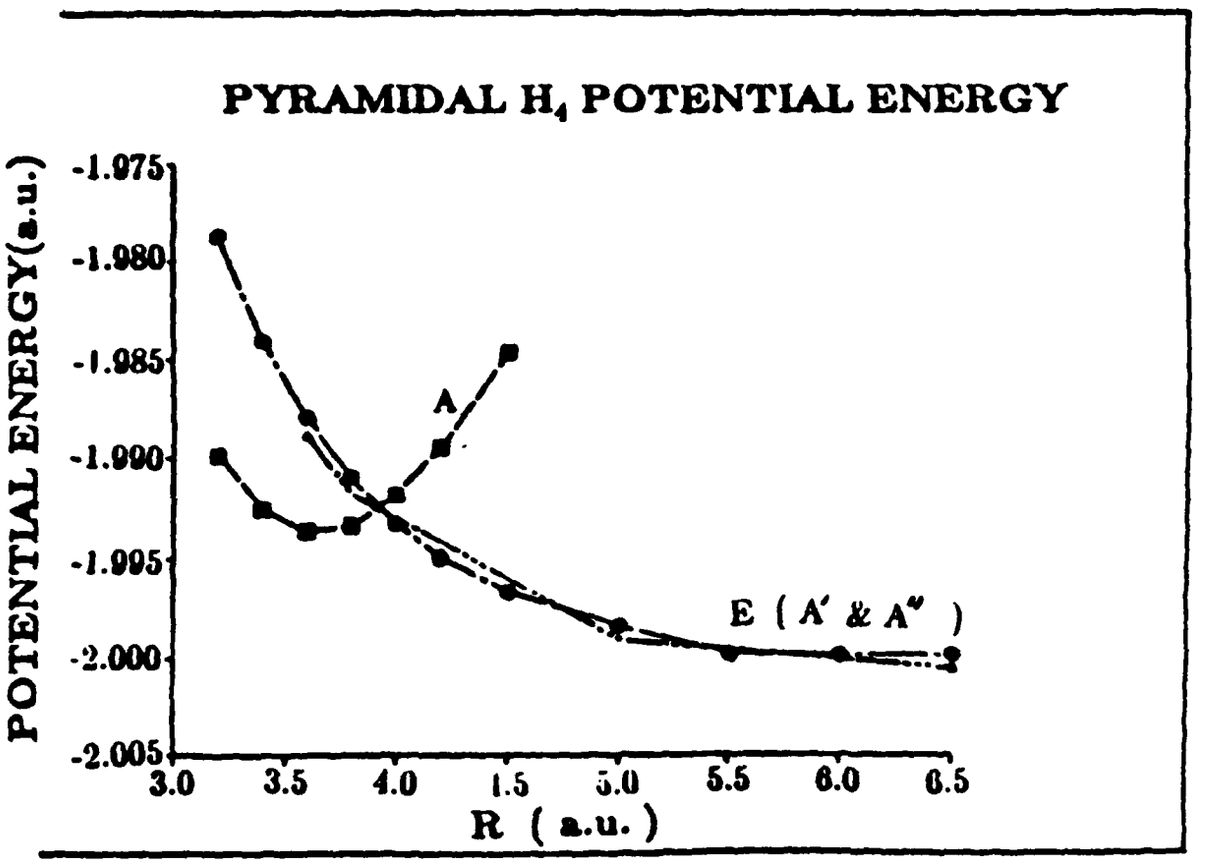

Figure 4. Potential energy curves from MCSCF trial functions for trigonal pyramidal geometry and C_{3v} symmetry (r = 1.70 a.u.). State designations for C_s symmetry are indicated in parentheses. The lack of coincidence of the degenerate E curves reflects their calculation in lower symmetry and provides an indication of MCSCF convergence.

Geometries and energies for the approach of $H_2(B)$ to $H_2(X)$

step	R′	L_1	L_2	$L_2(+)$	$L_2(-)$	D	energy lowing
I	5-2.2	1.40	2.43	1.215	1.215	0.0	-0.91
II	2.2	1.40	2.43	1.215-1.93	1.215-0.5	0.715	-0.20
III	2.2	1.60	2.63	1.93-2.13	0.5	0.865	-0.20
IV	2.2-1.75	1.60	2.63	2.14	0.5	0.865	-0.20
V	1.75-1.55	1.60	2.73	2.23	0.5	0.915	-0.46
VI	1.55	1.60	3.13	2.23-2.63	0.5	1.115	-0.69
VII	1.50	1.70	3.23	2.63-2.73	0.5	1.165	-0.11

TOTAL ENERGY LOWERING FOR THE SEVEN STEPS IS 3.75 ev.

* Distances in a.u.; energies in ev.

R′ - distance between the midpoint of $H_2(X)$ and the point where $H_2(B)$ meets the $H_2(X)$ plane.

L_1 - length of $H_2(X)$.

L_2 - length of $H_2(B)$.

$L_2(+)$ - length of $H_2(B)$ above $H_2(X)$ plane.

$L_2(-)$ - length of $H_2(B)$ below $H_2(X)$ plane.

D - magnitude of shift of $H_2(B)$ midpoint (above (+)/below(-)) plane of $H_2(X)$.

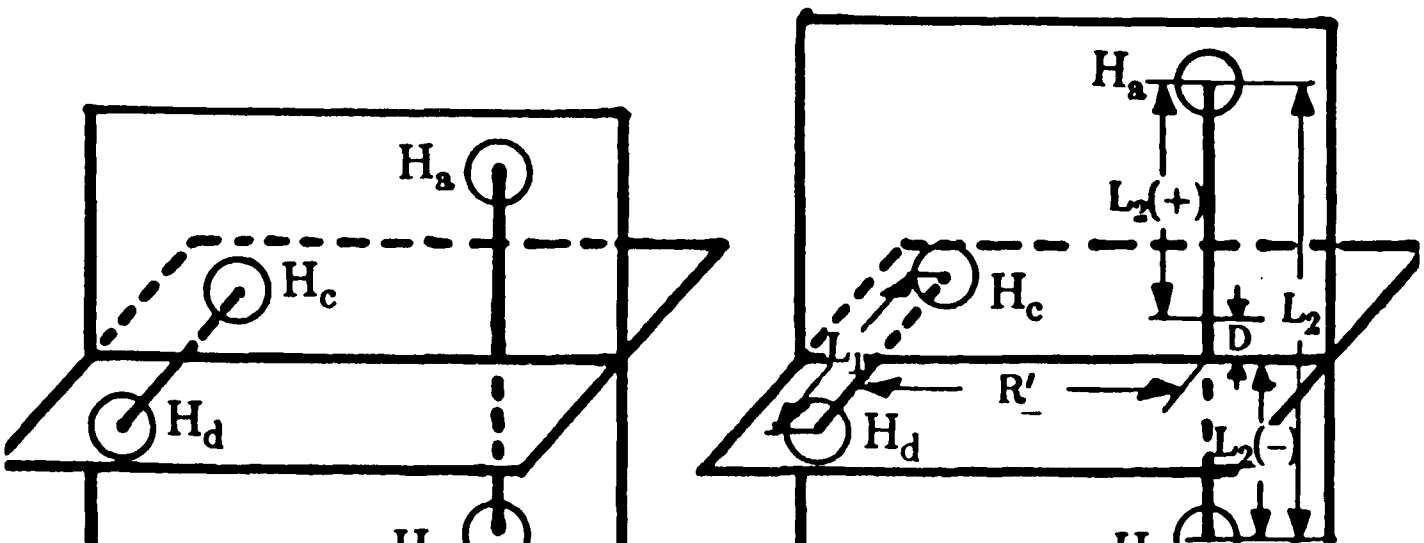

Figure 1. Geometries used to calculate the approach of $H_2(B)$ to $H_2(X)$.

asymptotic region to the neighborhood of the H_4 MIES configuration. The table also contains the energy lowering associated with the steps that are plotted in Fig. 6. It is noteworthy that no energy barrier is encountered along this path. Further, Fig. 7 show that when H(B) is displaced from bisecting H_2(X) in step II, charge transfer immediately occurs. (Similar behavior has been found for the related H_2(B) + He system in an independent study by WAL.)

FNQMC STUDY OF THE GROUND-STATE PYRAMIDAL STRUCTURE FOR C_{3v} SYMMETRY

FNQMC calculations using the MCSCF trial functions discussed above yield $\approx$ 0.6-1.0 eV energy lowering compared to the results of NTP and are presented in Fig. 8. Such a large change was not anticipated and so it was important to test the validity of this finding. To this end a configuration interaction calculation including all single and double excitations (SDCI) using the MCSCF pilot study basis set was carried out at R = 3.4 a.u. The energy was 0.32 eV lower than NTP's value and is consistent with the improvement expected based on studies of other systems. The FNQMC results of Fig. 8 obtained using a new trial function optimization algorithm, mentioned in the next section, are generally an improvement over those of Fig. 8 obtained using MCSCF trial functions.

FNQMC STUDY OF THE EXCITED STATE

These calculations provide the severest test of the FNQMC approach because of the lack of knowledge of the accuracy of the excited state trial function needed to provide a nodal description that assures orthogonality to the

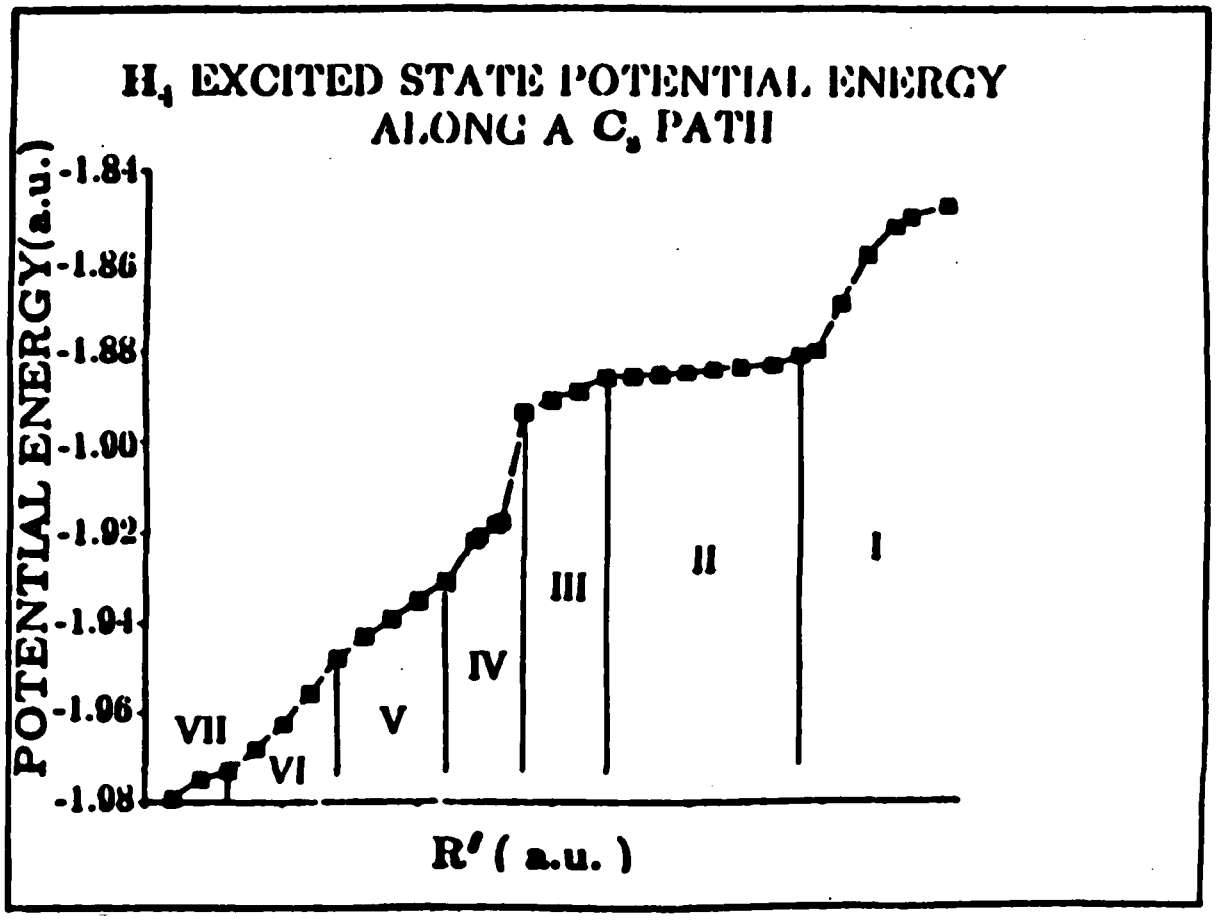

Figure 6. Plot of total energies corresponding to the pathway presented in Fig. 5.

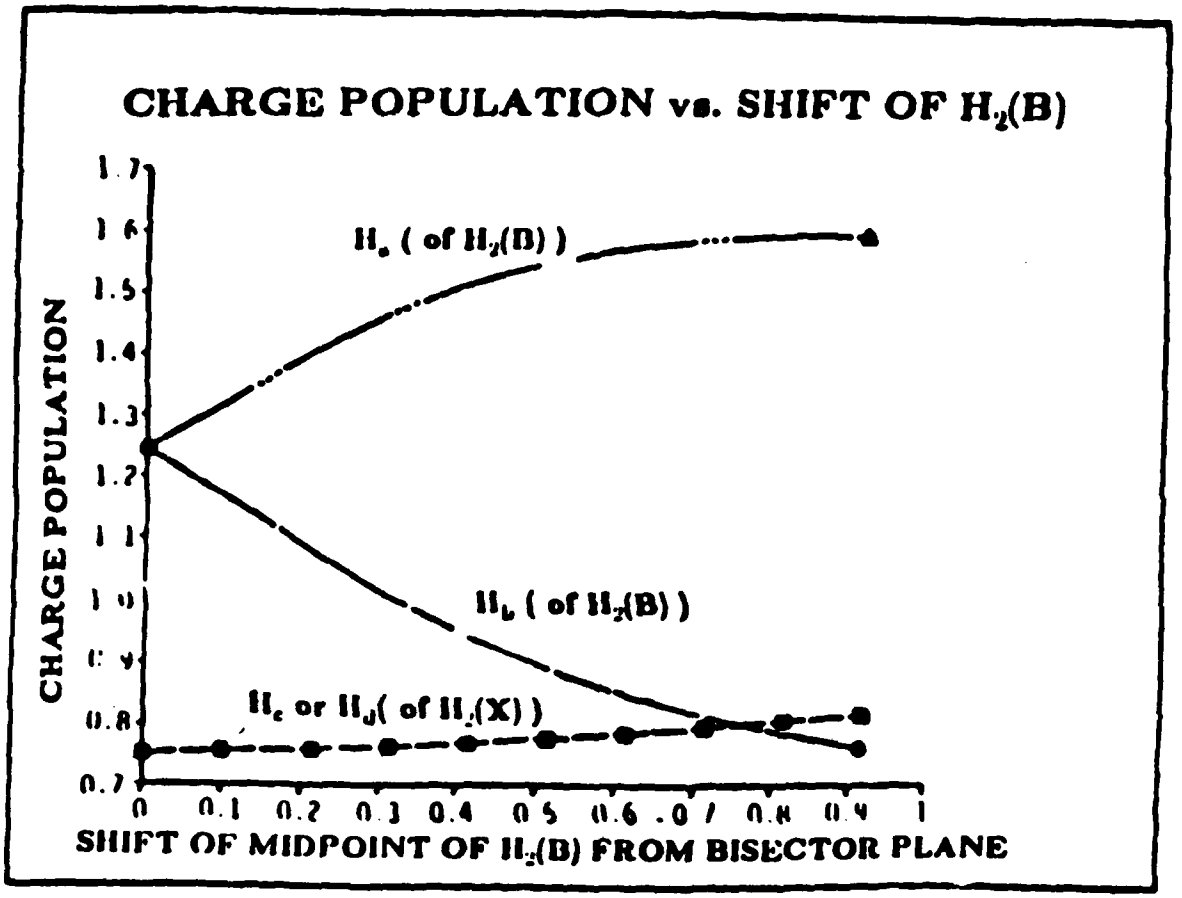

Figure 7. Change of charge distribution between H_a and H_b as a function of d, the displacement of the midpoint of $H_2(B)$ above the plane of $H_2(X)$.

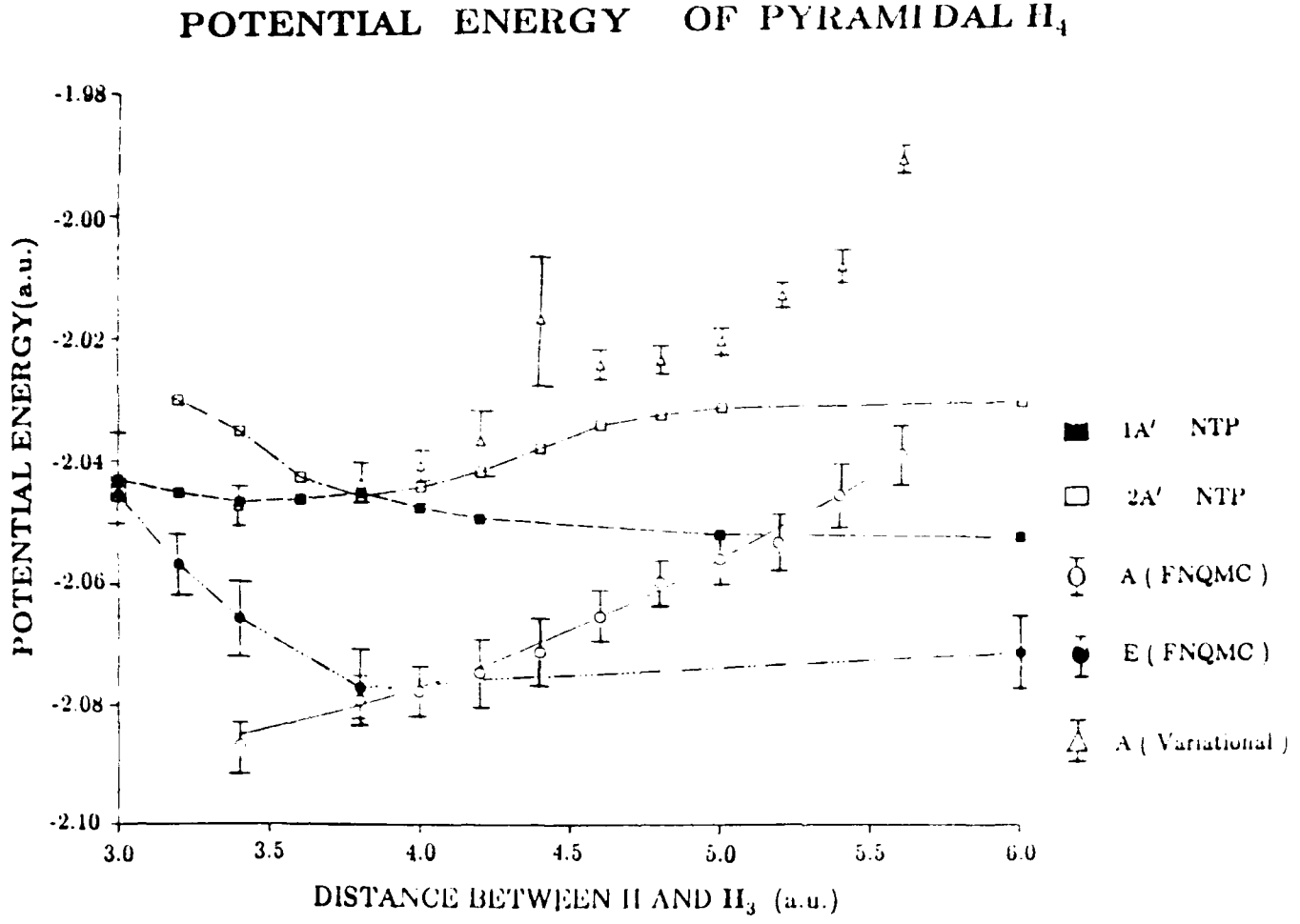

Figure 8. Potential energy of trigonal pyramidal H_4 versus R. The A (variational) results were determined using a new optimization method for QMC trial functions.

ground state of the same (A') symmetry (C_s). MCSCF calculations close to the avoided crossing suffered from root flipping. Despite the use of familiar MCSCF strategies to address the problem, it could not be resolved.

The MCSCF convergence problem had been encountered earlier for He + H_2(B) but resolved by the use of an *ab initio* CI method. Interest here in using the FNQMC method led us to develop a method for trial function construction[6] that avoids the MCSCF procedure. The approach amounts to the introduction of parameter optimization in the random walk process. Using group theory, a projection operator is constructed and used to constrain the wave function to have the symmetry properties of the state of interest. This method has been employed in the present effort to generate the A-state FNQMC results, denoted A(FNQMC), of Fig. 8. Calculations using this method are in progress to complete the E-state curve, labeled E(FNQMC), in Fig. 8 for $3.8 < R < 6.0$ a.u.

SA-MCSCF STUDY OF DISTORTED GEOMETRIES

Calculations have been carried out using the state averaged(SA)-MCSCF method to develop trial functions for a QMC study of the topography of the ground- and excited-state potential energy surface (pes) in the region of the symmetric geometry of the MIES determined by NTP. Figure 9 presents the coordinate system, Fig. 10 provides perspective views, and Fig. 11 (R = 4.0 a.u.) and Fig. 12 (R = 3.8 a.u.) show contour maps of the pes in the MIES region. Figures 11 and 12 show that the ground state has a saddle point at smaller R than the minimum of the excited state and that both features correspond to an isosceles triangle base for the MIES system. Further geometry optimization is

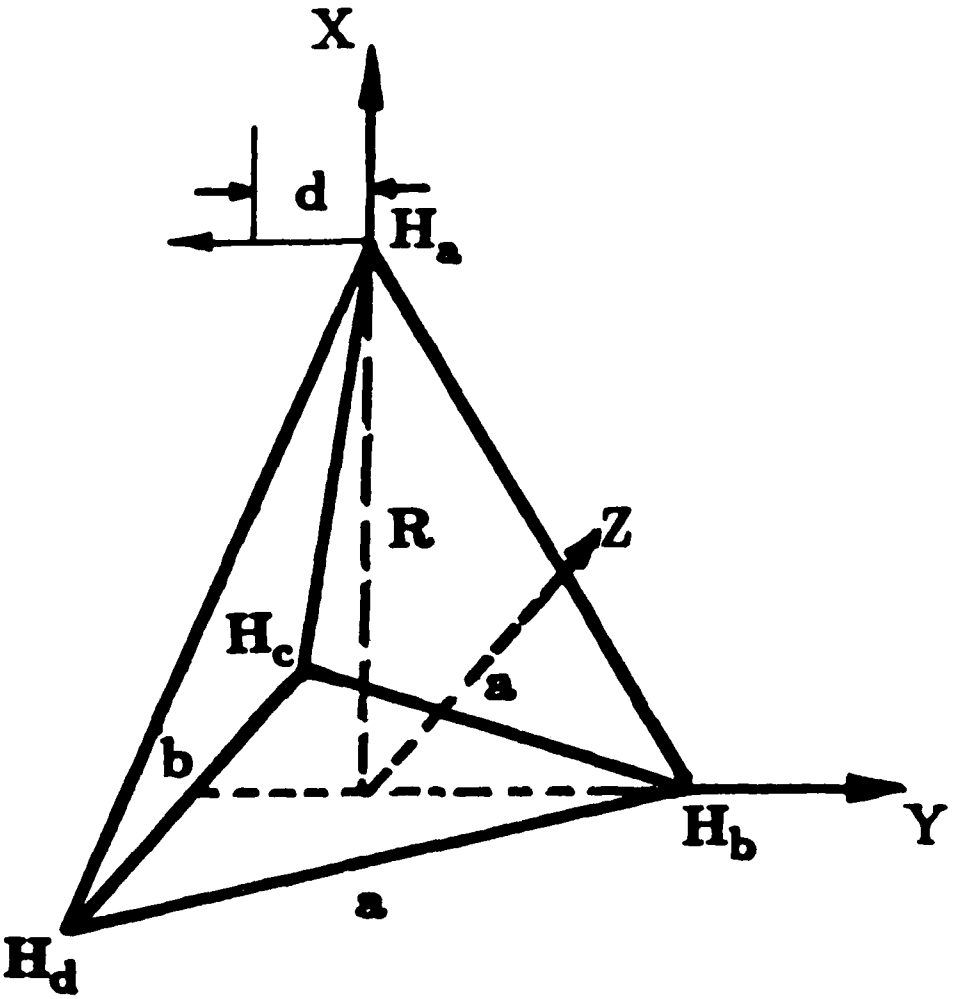

Figure 9. MIES coordinate system used for geometry variation. d is the magnitude of the displacement of H_a along the bisector of the H_cH_d side of length b.

H_4 3-D POTENTIAL ENERGY SURFACE (R=3.8 a.u.)

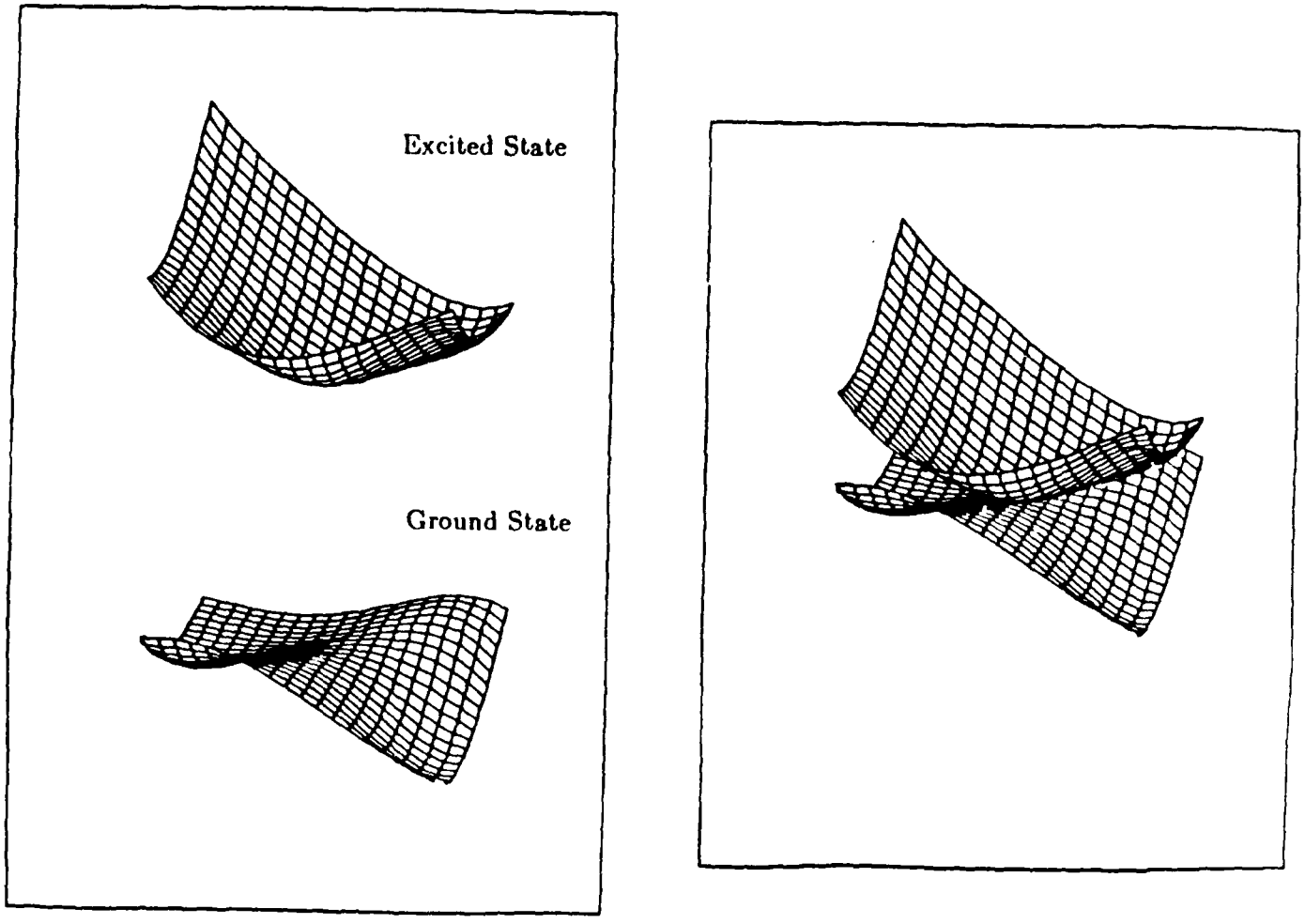

Figure 10. Potential energy surfaces for the ground- and excited-state separately for easy visualization and in computed relative positioning. Note the minimum of the excited state and saddle point of the ground state.

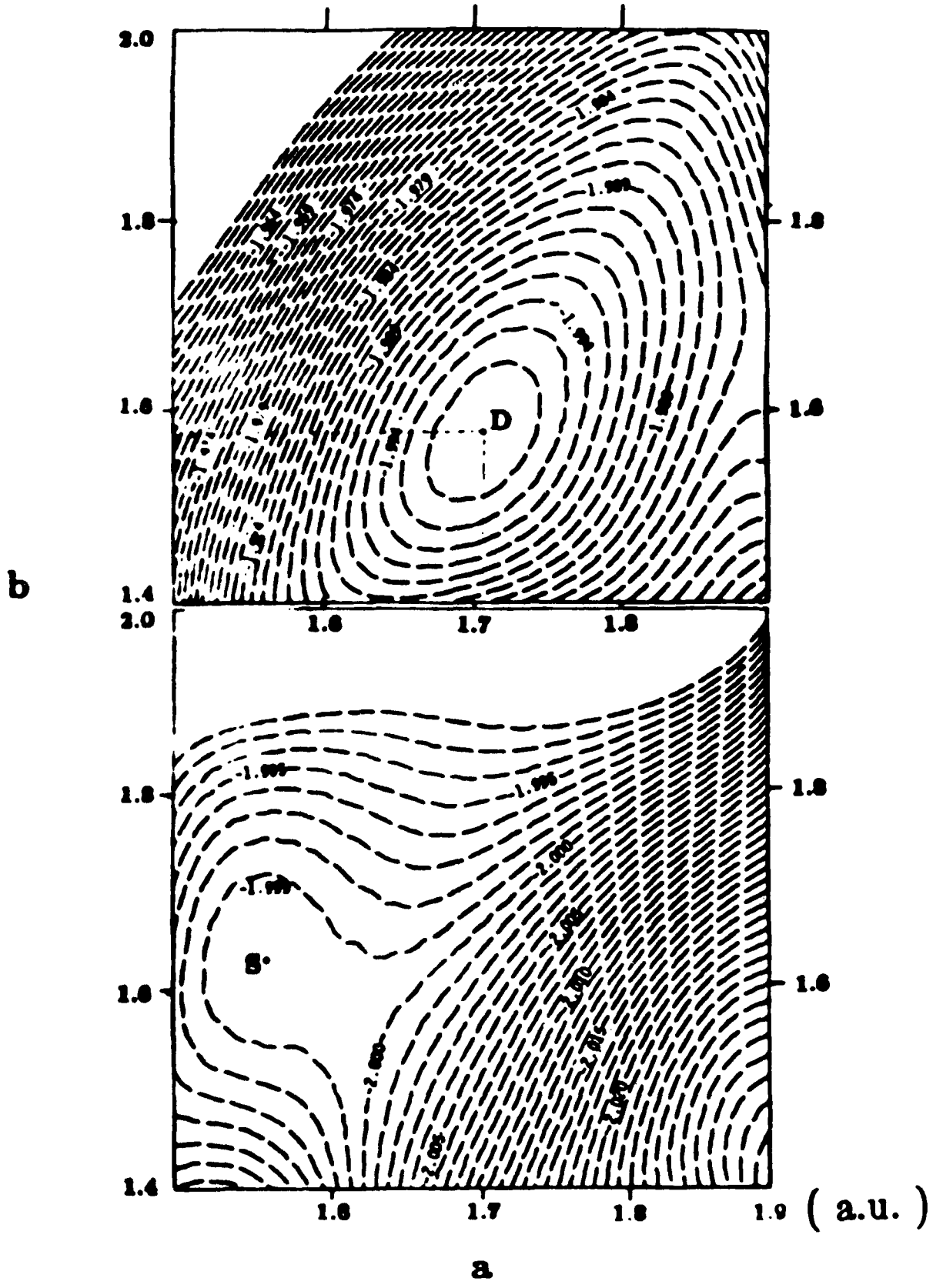

Figure 11. Potential energy contour [illegible]
as a function of r and b; see Fig. 9.

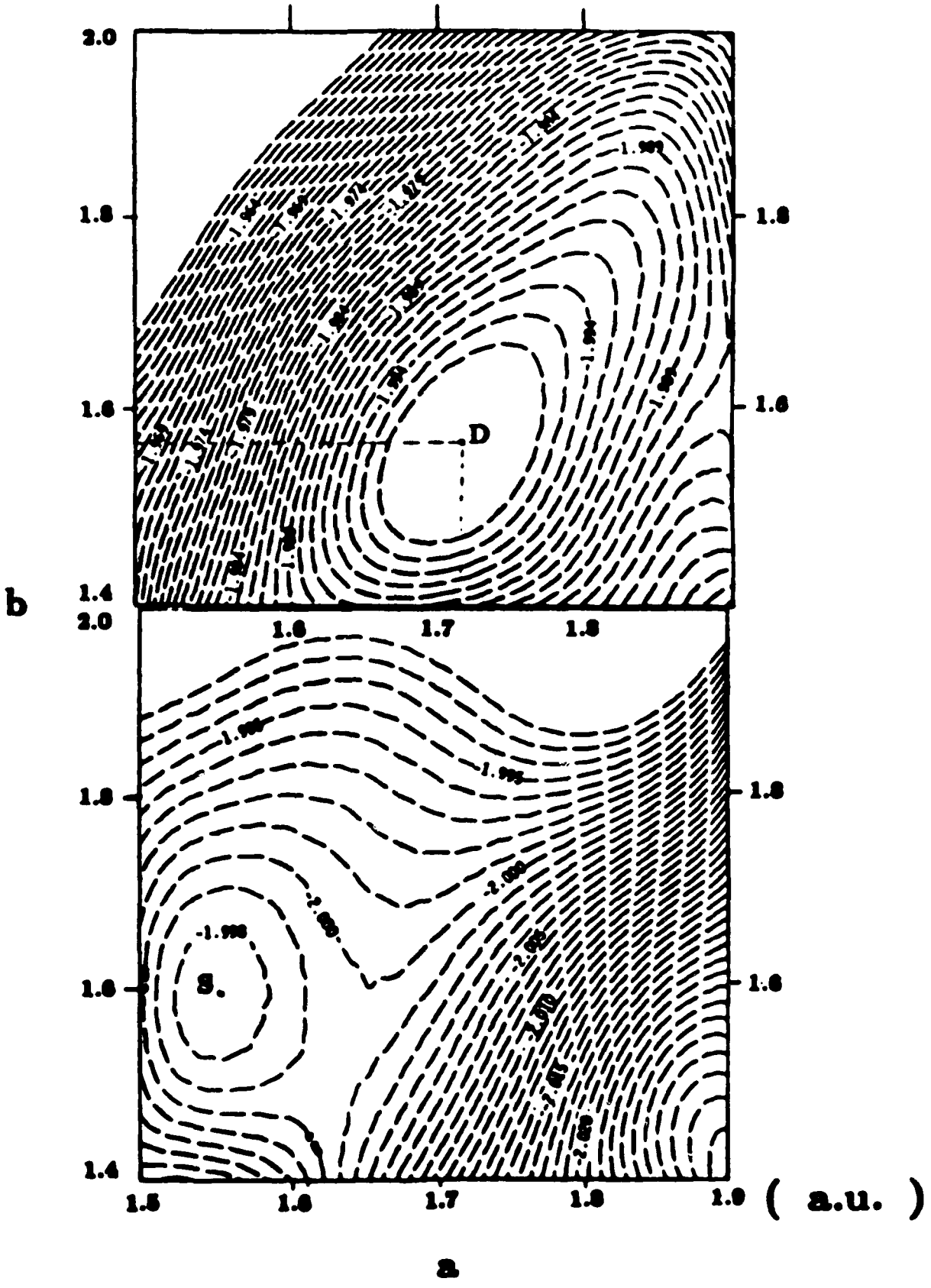

Figure 12. Same as Fig. 11 for E = 3.8 a.u.

POTENTIAL ENERGY V_s d

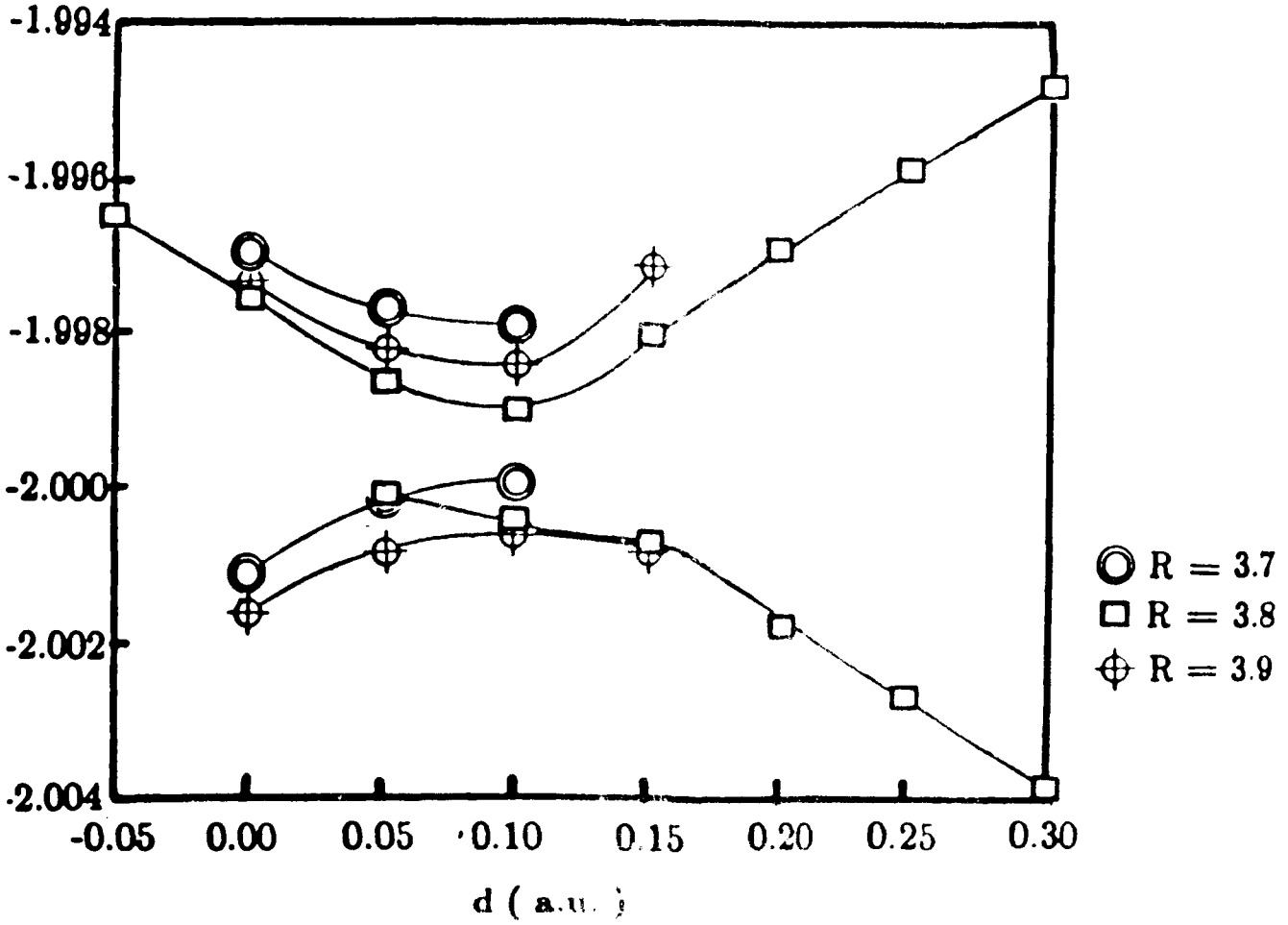

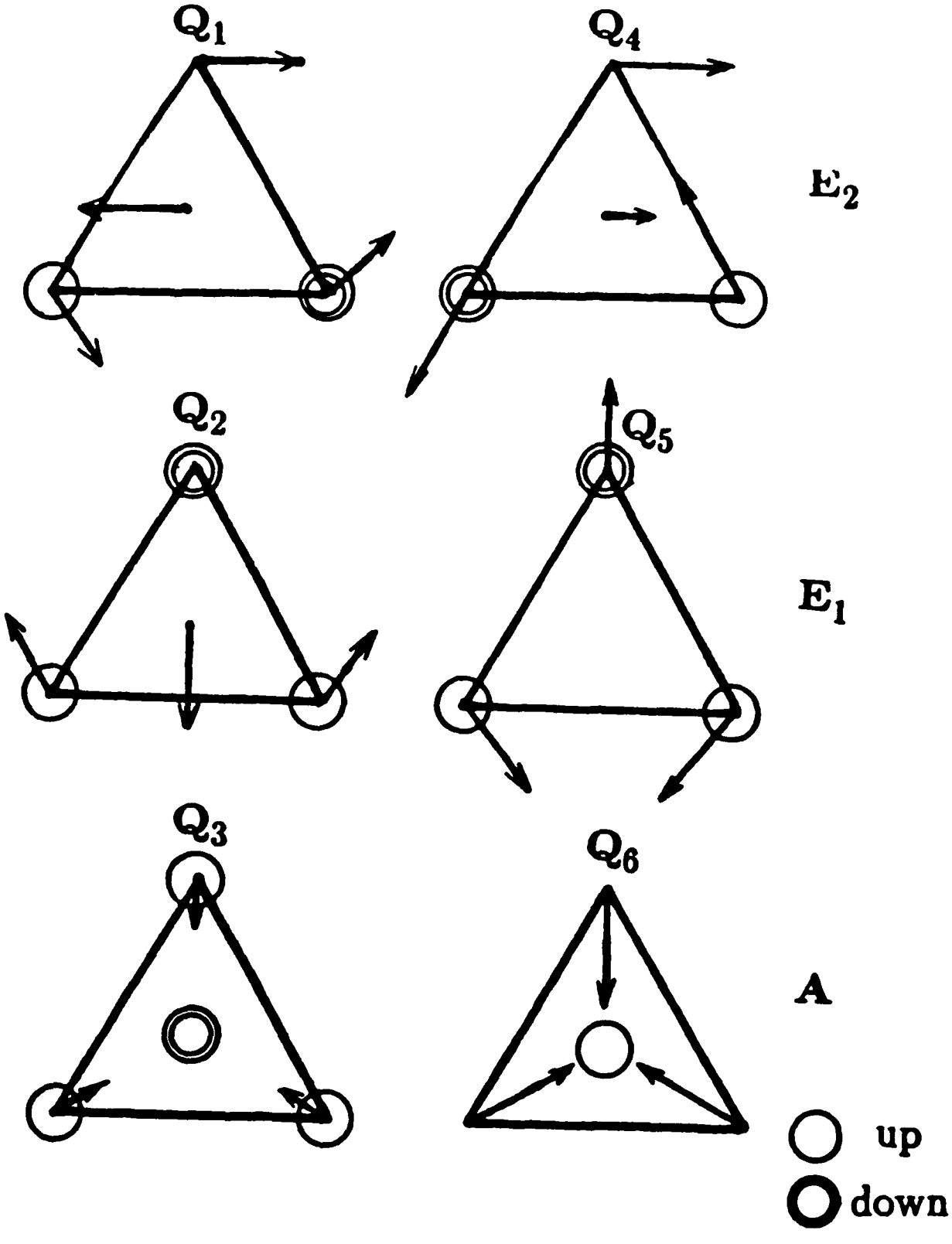

Figure 14. Normal mode displacement of H_4 in C_{3v} symmetry.

explored in Fig. 13 which plots potential energy as a function of d, the displacement of H_1 towards the base of the H_3 isosceles arrangement. The minimum for the excited state is found for d = 0.1 a.u.

NONADIABATIC COUPLING

The stability of the MIES system is dependent on nonadiabatic coupling (NAC) to the ground state. Although the focus of this study is characterization of the region of pes of the MIES, the need to ascertain first the stability of the excited system is a high priority here because of the effort associated with the trial function optimization method and the expense of QMC calculations with small statistical variances. To calculate the NAC matrix elements we took advantage of the simplications made possible by the use of normal mode distortions (Fig. 14) from the highly symmetric C_{3v} symmetry. Our calculation show that nuclear displacements associated with modes Q_1 and Q_2 lead to strong coupling between the A and E states. Relatively weaker coupling is found in Q_4 and Q_5. The two totally symmetric modes (Q_3 and Q_6) give no contribution.

The size of the NAC matrix elements connecting the A′ state to the E-state components (C_{3v} notation is used here to indicate parentage) are tabulated in Fig. 15 for the minimum energy geometry of the A state. These results establish that there is strong coupling between these states. Further computational study is needed to confirm these predictions and to estimate reliably the excited state lifetime.

Coupling matrix elements D^{CI} by a finite difference method (extrapolated from δQ = 0.002, 0.001, and 0.0005).

	$<E_2 \mid A' >$	$<E_1 \mid A' >$
Q_1	-2.0112(64)	0.0015(0)
Q_2	0.0017(0)	2.0127(98)
Q_3	0.0000	0.0000
Q_4	-0.3904(389)	-0.0010(3)
Q_5	-0.0039(13)	-0.3113(196)
Q_6	0.0000	0.0000

E_1 and E_2 are doubly degenerate states where E_1 is symmetric and E_2 is antisymmetric.

Figure 15. CI contribution to coupling matrix elements for normal mode displacement, see Fig. 14.

References

1. Nicolaides, C.A., Theodorakopoulos, G., and Petsalakis, I. D., J. Chem. Phys. vol. 80, pg. 1705 [1984].

2. Nicolaides, C. A. and Dzetsis, A., J. Chem. Phys. vol. 80, pg. 1900, [1984].

3. Nicolaides, C. A., Petsalakis, I. D., and Theodorakopoulos, G. J., Chem. Phys. vol. 81, pg. 748 [1984].

4. Reynolds, P. J., Ceperley, D. M., Alder, B. J., and Lester, W. A. Jr., J. Chem. Phys. vol. 77, pg. 5593, [1982].

5. Grimes, R. M., Hammond, B. L., Reynolds, P. J., and Lester, W. A. Jr., J. Chem. Phys. vol. 85, pg. 4749, [1986].

6. Sun, Z., Huang, S.-Y., and Lester, W. A. Jr., "*Algorithm for Optimizing Parameters in Quantum Monte Carlo Trial Function,*" to be published.

END

DATE

FILMED

MARCH

1988

DTIC